J. Biochem. **141,** 525–534 (2007)
doi:10.1093/jb/mvm054

Two Mutations Convert Mammalian Xanthine Oxidoreductase to Highly Superoxide-productive Xanthine Oxidase

Ryosuke Asai[1], Tomoko Nishino[1], Tomohiro Matsumura[1], Ken Okamoto[1], Kiyohiko Igarashi[2], Emil F. Pai[3] and Takeshi Nishino[1,*]

[1]Department of Biochemistry and Department of Molecular Biology, Nippon Medical School, 1-1-5 Sendagi, Bunkyo-ku, Tokyo 113-8602; [2]Department of Biomaterials Sciences, School of Agricultural and Life Sciences, The University of Tokyo, Bunkyo-ku, Tokyo 113-8657; and [3]Department of Biochemistry, Department of Medical Biophysics and Department of Molecular and Medical Genetics, University of Toronto and Division of Cancer Genomics and Proteomics, Ontario Cancer Institute/University Health Network, MaRS/TMDT, 101 College Street, Toronto, ON, Canada M5G 1L7

Received January 9, 2007; accepted January 30, 2007; published online February 14, 2007

Reactive oxygen species are generated by various systems, including NADPH oxidases, xanthine oxidoreductase (XOR) and mitochondrial respiratory enzymes, and contribute to many physiological and pathological phenomena. Mammalian xanthine dehydrogenase (XDH) can be converted to xanthine oxidase (XO), which produces both superoxide anion and hydrogen peroxide in a molar ratio of about 1:3, depending upon the conditions. Here, we present a mutant of rat XOR that displays mainly XO activity with a superoxide:hydrogen peroxide production ratio of about 6:1. In the mutant, tryptophan 335, which is a component of the amino acid cluster crucial for switching from the XDH to the XO conformation, was replaced with alanine, and phenylalanine 336, which modulates FAD's redox potential through stacking interactions with the flavin cofactor, was changed to leucine. When the mutant was expressed in Sf9 cells, it was obtained in the XO form, and dithiothreitol treatment only partially restored the pyridine nucleotide-binding capacity. The crystal structure of the dithiothreitol-treated mutant at 2.3 Å resolution showed the enzyme's two subunits to be quite similar, but not identical: the cluster involved in conformation-switching was completely disrupted in one subunit, but remained partly associated in the other one. The chain trace of the active site loop in this mutant is very similar to that of the bovine XO form. These results are consistent with the idea that the XDH and XO forms of the mutant are in an equilibrium that greatly favours the XO form, but the equilibrium is partly shifted towards the XDH form upon incubation with dithiothreitol.

Key words: superoxide, hydrogen peroxide, reactive oxygen species, xanthine oxidase, xanthine dehydrogenase, molybdenum cofactor.

Abbreviations: $ACPY^+$ and ACPYH, acetylpyridine adenine dinucleotide and its reduced form; AFR, activity-to-flavin ratio; $FADH^*$, FAD semiquinone; [2Fe–2S] and Fe/S, iron-sulphur cluster; KP buffer, potassium phosphate buffer; Sf9, cell line of *spodoptera frugiperda*; XOR, xanthine oxidoreductase; XDH, xanthine dehydrogenase; XO, xanthine oxidase.

Xanthine oxidoreductase (XOR) catalyses the oxidation of hypoxanthine to xanthine or xanthine to uric acid in the metabolic pathway of purine degradation (*1*, *2*). The animal enzymes are homodimers of molecular mass around 290 kDa, with each of the monomers acting independently during catalysis. Each subunit contains one molybdopterin cofactor, two non-identical [2Fe–2S] centres, and one flavin adenine dinucleotide (FAD) cofactor (*2*, *3*), which are located in the corresponding C-terminal 85 kDa, N-terminal 20 kDa and intermediate 40 kDa domains, respectively (*4–6*). The oxidation of xanthine takes place at the molybdopterin centre and the electrons thus introduced are rapidly transferred to FAD via the Fe/SI and Fe/SII centres (*7–10*). The reoxidation of the reduced enzyme by the oxidant substrate, NAD^+ or molecular oxygen, occurs through FAD (*10*, *11*). The enzyme from most organisms exists only in its xanthine dehydrogenase (XDH) form, in which it shows a preference for NAD^+ as the oxidizing substrate at FAD. However, mammalian XDHs can be converted to the xanthine oxidase (XO) form, which exclusively uses O_2 as its substrate (*12–14*). This conversion occurs either reversibly by formation of disulphide bridges or irreversibly by proteolytic cleavage within the XOR protein molecule (*2*, *12–19*). Reactive oxygen species (ROS), H_2O_2 and O_2^-, are formed when dioxygen is used as the substrate, and the enzyme in endothelial cells (*20*) has been implicated in diseases characterized by oxygen radical-induced tissue damage, such as post-ischaemic reperfusion injury (*21–24*).

The crystal structures of both the XDH and XO forms of the enzyme from bovine milk have been determined and the structural differences between the two forms

*To whom correspondence should be addressed. Tel: +81-3-3822-2131, Fax: +81-3-5685-3054, E-mail: nishino@nms.ac.jp

have been described (*6*). Based on site-directed mutagenesis studies of rat XOR expressed in a *Spodoptera frugiperda* (Sf9)/insect cell system, the two disulphide bonds responsible for the reversible conversion were identified as Cys535–Cys992 and Cys1316–Cys1324 (*25*). The former bond forms rapidly, whereas the latter one forms much more slowly, based on chemical modification studies with 2-fluorodinitrobenzene or 4,4′-dithiodipyridine (*25*). In the crystal structure, Cys535 is located on the long linker peptide between the FAD and molybdopterin domains, whereas Cys992 is found on the surface of the molybdopterin domain (*25*). The site of proteolytic cleavage responsible for irreversible conversion is in the same linker peptide (*6*). A mechanism for the transition from XDH to XO has been proposed based on a detailed comparison of the XDH and XO structures, including the results of site-directed mutagenesis studies (*25*, *26*). Mechanistic models focus on an amino acid cluster formed by the residues Arg334, Trp335, Arg426 and Phe549 (amino acid numbers are those for the rat enzyme). Held together mostly by π-cation interactions, this cluster sits at the centre of a relay system that can transmit modifications of the linker peptide, e.g. disulphide formation or proteolytic cleavage, to the FAD-approaching active site loop (rat enzyme Gln422-Lys432) (*6*), resulting in a dramatic change of the loop's conformation, as well as of the electrostatic environment around FAD (*6*). During these conformational transitions, the cluster acts not only as a transmitter, as described earlier, but also as a solvent gate (*26*). Obviously, tight interactions between the amino acid residues of the cluster are crucial for the stabilization of the XDH form of the enzyme. These interactions are disrupted, however, when Phe549 is removed from the cluster, either by a change in conformation induced by disulphide formation between Cys535 and Cys992, or by release of the linker peptide through proteolysis. It is highly likely that this disruption is the trigger for all subsequent rearrangements (*6*, 26). While the active site loop is close to the *si*-face of the flavin cofactor, the side chain of Phe336 stacks to the *re*-face of the isoalloxazine ring (*6*). As this π–π interaction seems to modulate the redox potentials of the flavin cofactor, removal of the aromatic ring in the mutant can be expected to change the character of the reactivity towards oxygen.

Although ROS are known to be formed in various systems, including NADPH oxidase (*27*) and mitochondrial respiratory enzymes (*28*), and they are considered to be involved in various physiological and pathological phenomena, there is no experimental system available for easy and reliable formation of O_2^-. This is mainly due to the complexity of the presently used systems, e.g. NADPH oxidase usually requires various activating cofactors (*27*). XO is frequently used as a tool for O_2^- production. The major problem in using XO as O_2^- generating tool, however, is that this enzyme is normally in its dehydrogenase form, and the formation of O_2^- is blocked by NAD^+, which is always present in large amounts even under anoxic conditions (*29*). Furthermore, even in the XO form of the native enzyme, only 15–20% of the total electrons are used to generate O_2^-, while the remaining electrons contribute to the unwanted formation of H_2O_2 (*17*).

Based on our structural and mechanistic studies of XOR enzymes (*6*, *26*), we set out to improve the superoxide-producing ability of the XOR system by creating the W335A/F336L double mutant of the rat enzyme. The first mutation led to the disruption of the key amino acid cluster (favouring the XO over the XDH structure), while removal of the π–π interaction at the FAD site by means of the second mutation dramatically increased the yield of O_2^-. Kinetic analysis showed that the double mutant mainly used molecular oxygen as the electron acceptor, regardless of the oxidation state of the crucial cysteine residues; in addition, the mutant's O_2^- yield was dramatically increased compared with that of active XO. The double mutant should prove very useful as a superoxide-generating tool. To further characterize the changes induced by these mutations, we crystallized the protein in the presence of dithiothreitol (DTT) and determined its crystal structure at 2.3 Å resolution.

EXPERIMENTAL PROCEDURES

Materials—Spodoptera frugiperda (Sf9) cells were obtained from Invitrogen (CA, USA) and BacVector™-2000 triple cut virus DNA was from Novagen (WI, USA). The transfer vector pJVP10Z was kindly provided by Dr Palmer Taylor (University of California, San Diego, CA, USA). Restriction and modification enzymes were from Takara Bio Inc. (Shiga, Japan) or New England Biolabs Inc. (MA, USA). The culture medium Sf-900II and Grace medium were purchased from Invitrogen, and fetal bovine serum from Hyclone (UT, USA). The polyclonal antibody used in these experiments was raised in our laboratory against purified rat liver XOR, as described previously (*4*). Materials and methods used for enzyme purification were described previously (*30*). All other chemicals were of reagent grade.

Preparation of the Transfer Vector for Expression of Mutant XOR, W335A/F336L—Site-directed mutagenesis was done using a QuickChange site-directed mutagenesis kit (Stratagene; CA, USA). To prepare the mutant cDNA of W335A/F336L (the codons for Trp335 and Phe336 are replaced with the codons for Ala and Leu, respectively), the mutagenic PCR reaction was carried out using the plasmid pRXD203 as a template. The plasmid pRXD203 contains full-size rat XOR cDNA. Mutagenic oligonucleotide primers for W335A/F336L were as follows; forward primer, 5′-G GAG CAG CTG CGC GCG CTT GCC GGC AAG CAG G-3′, reverse primer, 5′-C CTG CTT GCC GGC AAG CGC GCG CAG CTG CTC C-3′. The plasmid of the W335A/F336L mutant, pRXD203-W335A/F336L, was sequenced to verify the presence of the desired mutations. DNA sequencing was performed with an ABI PRISM 310 Genetic Analyzer using a BigDye® Terminator Cycle Sequencing Ready Reaction sequencing kit (Applied Biosystems, CA, USA). The DNA fragment encoding the double mutant enzyme was excised with *Nhe*I from pRXD203-W335A/F336L plasmid, and cloned into the *Nhe*I site of baculovirus transfer vector pJVP10Z (*25*, *26*, *31*). The direction of the insert DNA was verified by DNA sequencing.

Construction of Recombinant Viral Variant—The recombinant virus was prepared as described previously

(*31*). Co-transfection of BacVector™-2000 triple cut virus DNA and constructed transfer vector was conducted using Eufectin™ Transfection Reagent (Novagen); screening of the recombinant virus was carried out by plaque assay according to the manufacturer's manual (*31–33*). To identify recombination, direct western blots were performed with infected cell extracts of the second virus amplification and positive clones were selected. Usually, virus stock with a titre of 1×10^7 plaque-forming units/ml or more was prepared.

Overexpression of the Mutant Using the Baculovirus–Insect Cell System—The maintenance of Sf9 cell lines and the expression procedures were the same as described previously (*31*).

Purification Procedures for Recombinant Enzymes—Recombinant enzyme was purified as described previously (*31*); the recombinant active XOR and demolybdo-dimeric XOR were separated by affinity column chromatography (*30*, *34*). The enzymes were concentrated and incubated with 5 mM DTT for 1 h at 25°C to generate the XDH form of XOR, if necessary.

Enzyme Assays—Enzyme assays were carried out at 25°C in 50 mM potassium phosphate (KP) buffer (pH 7.8) containing 0.4 mM EDTA in the final volume of 1.0 ml. XOR activities with various electron acceptors were determined by monitoring the absorbance changes as follows: O_2 (air-saturated buffer; 295 nm), NAD^+ (500 μM; 340 nm), $ACPY^+$ (500 μM; 360 nm). The extinction coefficients of 6.22 $mM^{-1}cm^{-1}$ for NADH and 9.1 $mM^{-1}cm^{-1}$ for ACPYH were used. Concentration of the mutant enzyme was determined from the absorbance at 450 nm using an extinction coefficient of 35.8 $mM^{-1}cm^{-1}$ (*35*). Activity-to-flavin ratio (AFR) (*1*) was obtained by dividing the change in absorbance/min at 295 nm in the presence of NAD^+ under aerobic conditions by the absorbance at 450 nm of the enzyme used in the assay at 25°C. Photometric experiments were performed with a UV-2550 spectrophotometer (Shimadzu, Kyoto, Japan) equipped with a temperature-control system.

Steady-state Kinetics of Xanthine–O_2 Activity—2.5 ml of the reaction mixture contained 50 mM KP buffer pH 7.8, 0.4 mM EDTA, 0.15 mM xanthine (fixed concentration) and 14 nM of the double mutant with or without DTT treatment. Before the addition of the enzyme, the incubation mixture was bubbled with nitrogen gas containing various concentrations of oxygen (5.35, 10.2, 15.4, 21.0 or 50.8% O_2) for 5 min at 25°C in an anaerobic cuvette equipped with an enzyme injector. After the addition of the enzyme, the absorbance at 295 nm was followed at 25°C with a UV-2550 spectrophotometer (Shimadzu).

Determination of Uric Acid and O_2^- during Xanthine–O_2 Turnover—Formation of O_2^- was estimated in terms of reduction of cytochrome *c*, following the method of McCord and Fridovich (*36*). Reduction of cytochrome *c* was followed at 550 nm: the concentration of O_2^- was estimated from the Δe_{550} value between the reduced and oxidized cytochrome *c* of $2.1 \times 10^4\,M^{-1}\,cm^{-1}$ (*37*). Formation of uric acid was determined by following the absorbance change at 295 nm, using a Δe_{295} value between uric acid and xanthine of 9.6 $mM^{-1}cm^{-1}$ (*5*). Correction was made for the absorbance change at 295 nm due to the reduction of cytochrome *c*. The Δe_{295} value of reduced–oxidized cytochrome *c* was 4.2 $mM^{-1}cm^{-1}$ (*5*).

Absorbance Spectra of the W335A/F336L Mutant during Anaerobic Reduction with NADH—The DTT-treated double mutant enzyme (4.6 μmol) in 50 mM KP buffer (pH 7.8) containing 0.4 mM EDTA was mixed with 1/39 volume of NADH (5.08 mM) under anaerobic conditions. Absorption spectra were recorded at the times indicated using a DU-7400 spectrophotometer (Beckman Coulter, CA, USA).

Rapid Reaction Kinetics of the W335A/F336L Mutant—Rapid half-reaction experiments were carried out under anaerobic conditions in 50 mM KP buffer (pH 7.8) containing 0.4 mM EDTA at 25°C with an SX-18MV kinetic spectrophotometer (Applied Photophysics Ltd, UK) with a 1 cm observation path length. A 75 μl aliquot of this solution containing the double mutant at a concentration of 7.5 μM was mixed with an equal volume of various concentrations of NADH. Absorbance changes were monitored at 450, 520 and 620 nm in time periods ranging from the dead-time (about 2 ms) to 1 s, and the observed rate constants k_{obs} were then plotted against substrate concentration to obtain the reduction constant (k_{red}) and the dissociation constant (K_d) (*38*).

Crystallization of the W335A/F336L Mutant of Rat XOR and Collection of Diffraction Data—The methods of enzyme preparation for crystallization were the same as described previously (*25*). The enzyme was concentrated to 8 mg/ml in a buffer mixture of 15% 0.1 M pyrophosphate (pH 8.5) containing 0.2 mM EDTA and 85% 0.05 M KP buffer (pH 7.4) containing 0.2 mM EDTA and incubated with 5 mM DTT for 60 min at 25°C. Crystals of the W335A/F336L mutant XDH were grown by vapour diffusion, equilibrating a mixture of 1 μl of protein and 1 μl of reservoir solution containing 9–10.5% polyethylene glycol 8000, 0.6 M lithium sulfate, 5 mM DTT, 1 mM sodium salicylate, 0.4 mM EDTA, 15% glycerol and 40 mM HEPES (pH 6.2), against 1.5 ml of reservoir solution. Crystals of the enzyme were flash-frozen with their mother liquor as a cryoprotectant and mounted in cryoloops (Hampton Research CA, USA). A crystal was placed in a nitrogen stream at 100 K and diffraction data were collected at a wavelength of 1.00 Å on beamline BL38B1, Spring-8 (JASRI, Hyogo, Japan) using a Q4 area detector (Area Detector Systems Corporation).

RESULTS

Expression and Purification of the W335A/F336L Mutant of Recombinant Rat Liver XOR—In an effort to generate a form of XOR that would preferentially produce superoxide in high yield and independently of the presence or absence of thiol reagents, we constructed the W335A/F336L double mutant and expressed it in the baculovirus–Sf9 insect cell system. In this system, co-formation of catalytically inactive demolybdo-monomeric and -dimeric forms, as well as active and inactive molybdo forms, is unavoidable (*31*). In this study, we used the molybdo forms (both active and inactive) as they were eluted from the first folate affinity

chromatography column. This column removes the demolybdo form only, so the resulting protein was suitable for functional analyses of the mutant enzyme. The only exception was in experiments to measure NADH reduction, in which the presence of the demolybdo form does not influence the results (*31*). At this step in the purification scheme, the active form of the enzyme showed an AFR at 25°C of 98 to 145, corresponding to 49–73% of the molecules being catalytically competent, since the AFR for the fully active enzyme is 200 (*17*, *34*). The most probable cause of the reduced activity is the presence of desulfo enzyme, as was shown earlier for the natural enzyme (*30*). When wild-type rat XOR is expressed in the baculovirus-Sf9 insect cell system, it is in the XDH form, which is then gradually converted to the oxidase form. The W335A/F336L mutant, however, was already expressed almost exclusively in its oxidase form and could be identified as such in the crude extract. The XO activity was not due to proteolytic cleavage, which would irreversibly generate this form of the enzyme; the protein eluted from the first folate affinity column showed a single band on SDS-PAGE corresponding to a molecular mass of 150 kDa (Fig. 1D).

DTT Treatment of Purified Enzyme—In wild-type XOR, any oxidatively generated XO (due to disulphide formation) can be converted to XDH in less than an hour by treating it with 5 mM DTT at 25°C (*25*). When the W335A/F336L mutant was expressed as the oxidase form, a situation seen before with the bovine W336A (corresponding to rat W335A) mutant (*26*), it was also incubated with DTT under the same conditions. In contrast to native (*17*) or expressed wild-type enzyme (*25*), however, the mutant was largely resistant to the conversion. Xanthine–O_2 activity (formation of urate in the absence of NAD^+) decreased only very slowly to reach about 70% of the initial activity after 60 min, with no further change observed thereafter. The xanthine–NAD^+ activity of the mutant increased only slightly (~15%) within the same time frame (Fig. 1A). These results indicated that only a small part of the mutant enzyme could be converted back to the XDH form by DTT treatment; the majority of molecules remain in the XO form. The lower urate formation activity found in the presence of NAD^+ than in the absence of NAD^+ can be explained by the inhibitory effect by NAD^+, which can bind to the pyridine nucleotide binding site partially reconstituted during DTT incubation, combined with the reduction of electron transfer from FAD to NAD^+ caused by the higher redox potential displayed by FAD in this mutant environment. The smaller increase of xanthine–NAD^+ activity (~15%) compared with the decrease of xanthine–O_2 activity (~30%) (urate formation in the absence of NAD^+) is also consistent with the positive shift of the redox potential of the FAD cofactor; when acetylpyridine adenine dinucleotide ($ACPY^+$), whose redox potential is ~60 mV more positive than that of NAD^+ (*39*), was used as an electron acceptor, the increases of xanthine–$ACPY^+$ activity and XO activity become comparable (Fig. 1B). It should also be noted that urate formation catalysed by the mutant was higher in the presence of $ACPY^+$ (Fig. 1B) than NAD^+ (Fig. 1A),

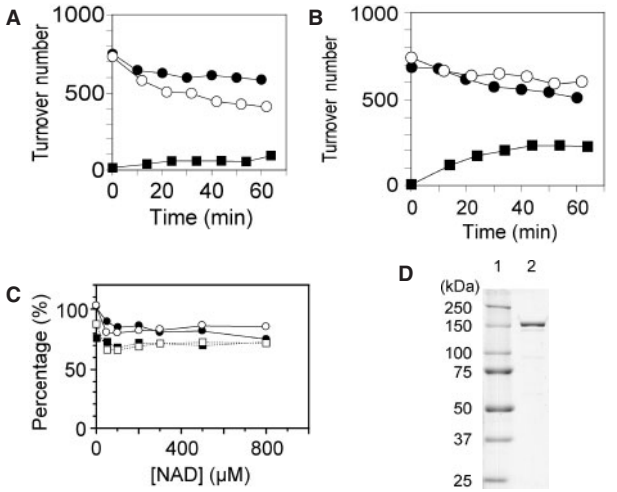

Fig. 1. **Time course of XDH/XO conversion of W335A/F336L mutant enzyme by incubation with dithiothreitol**. Freshly purified enzyme was incubated with 5 mM DTT at pH 7.8 and 25°C. During incubation, aliquots were withdrawn from the mixture to measure the enzyme activities. The activities are shown as turnover numbers (mols/mol FAD/min) corrected for the measured value of AFR, assuming an AFR value of 200 for the fully active enzyme (*16*). (A) Urate formation was determined by following absorbance changes at 295 nm in the absence (closed circle) the presence (open circle) of NAD^+ as described in Experimental Procedures. NADH formation activity was also determined by following absorbance changes at 340 nm in the presence of NAD^+ (closed square). (B) Urate formation determined at 295 nm in the absence (closed circle) or the presence (open circle) of $ACPY^+$. ACPYH formation was followed at 360 nm in the presence of $ACPY^+$ (closed square). (C) Cytochrome c reduction determined at 550 nm with the DTT treated (closed circle) or untreated enzyme (open circle). The O_2 flux represents the ratio of formation of O_2^- per total electrons provided to the the DTT treated (closed square) or untreated enzyme (open square). The O_2 flux represents the ratio of formation of O_2^- per total electrons provided to the enzyme in the presence (closed square) or the absence of NAD^+ (open square). (D) SDS-PAGE of purified W335A/F336A mutant. Lane 1, Marker proteins (Bio-Rad) having molecular masses of 250, 150, 100, 75, 50, 37 and 25 kDa. Lane 2, W335A/F336L mutant.

in accordance with the more efficient electron transfer occurring with $ACPY^+$ as the acceptor.

Steady-state Kinetics of Xanthine–O_2 Activity and Formation of O_2^-—The steady-state kinetics of xanthine–O_2 activity of the mutant was evaluated before and after DTT treatment with varying concentrations of oxygen and xanthine at a constant concentration of 0.15 mM electron donor. The apparent k_{cat} value of the mutant was comparable with that of native rat XO before DTT treatment, but decreased to 78% of its value after DTT treatment (Table 1). The K_m values for O_2 as a substrate were similar irrespective of exposure to DTT, again supporting the XO-like behaviour of the mutant. We determined the reduction rate of cytochrome *c* with xanthine as the electron donor in the presence and absence of superoxide dismutase to measure the O_2 flux ratio, i.e. the ratio of formation of O_2^- per total electrons provided to the enzyme. The percentages of one-electron transfer to O_2 were similar irrespective of DTT treatment

(Table 1). The values obtained with the mutant (~75%) were much higher than those with native enzyme from rat liver: the values with native enzyme were ~35% and ~15% for DTT-treated and untreated enzyme, respectively (*17*). The estimated molar production ratio of O_2^-: H_2O_2 in the mutant enzyme was 6:1, much higher than the value for native rat XO (1:3) determined under the same conditions (*17*). Thus, the mutant enzyme mainly used molecular oxygen as an electron acceptor and most of the electrons it received were used to produce O_2^-. As indicated in the previous section, the mutant seemed to partially retain its NAD^+ binding site; we, therefore, tested whether NAD^+ influences O_2^- production in both the DTT-treated and untreated mutant. As is the case with xanthine–O_2 activity, NAD^+ partly inhibited the formation of O_2^- activity, but the ratio of O_2^-: H_2O_2 formation was not significantly influenced by up to 800 μM NAD^+ (Fig. 1C).

Table 1. **Effects of dithiothreitol treatment on xanthine–O_2 activity and formation of O_2^- of theW335A/F336L mutant.**

	After purification (DTT untreated)	After DTT treatment
k_{cat} (moles of formed urate/min/mol of FAD-enzyme)	748 ± 17	584 ± 15
K_m for O_2 (μM)	129 ± 10	129 ± 9
k_{cat} for O_2^- formation (mols of reduced cytochrome *c*/min/mol of FAD-enzyme)	1110 ± 13	870 ± 20
O_2^- Flux (%)	74.4 ± 1.2	74.5 ± 1.2

k_{cat} and K_m values were determined at pH 7.8 and 25°C as apparent values with the concentration of xanthine fixed at 0.15mM. k_{cat} values were calculated for the used enzyme having an AFR value 136, assuming an AFR value of 200 for the fully active enzyme. O_2^- formation activity was determined by following the rate of cytochrome *c* reduction in the presence and absence of superoxide dismutase.

Reduction of DTT-treated Mutant Enzyme with NADH—As already mentioned the DTT-treated double mutant seemed to possess a partially folded NAD^+ binding site. Although NAD^+ is not a good electron acceptor because of the positive shift of the redox potential experienced by the reduced FAD cofactor in the mutant environment, NADH should be a good reductant of FAD. Figure 2A shows the reduction of the DTT-treated double mutant with NADH under anaerobic conditions. The DTT-treated mutant enzyme was apparently reduced by NADH in a biphasic manner: we observed fast reduction (within 20 s) followed by a second process (20 s–60 min). We interpret the latter as intermolecular reduction of non-NADH-reducible enzyme by NADH-reducible enzyme, a process frequently observed in XOR. After 20 s, the level of reduction was more than that of the bovine single mutant W336A

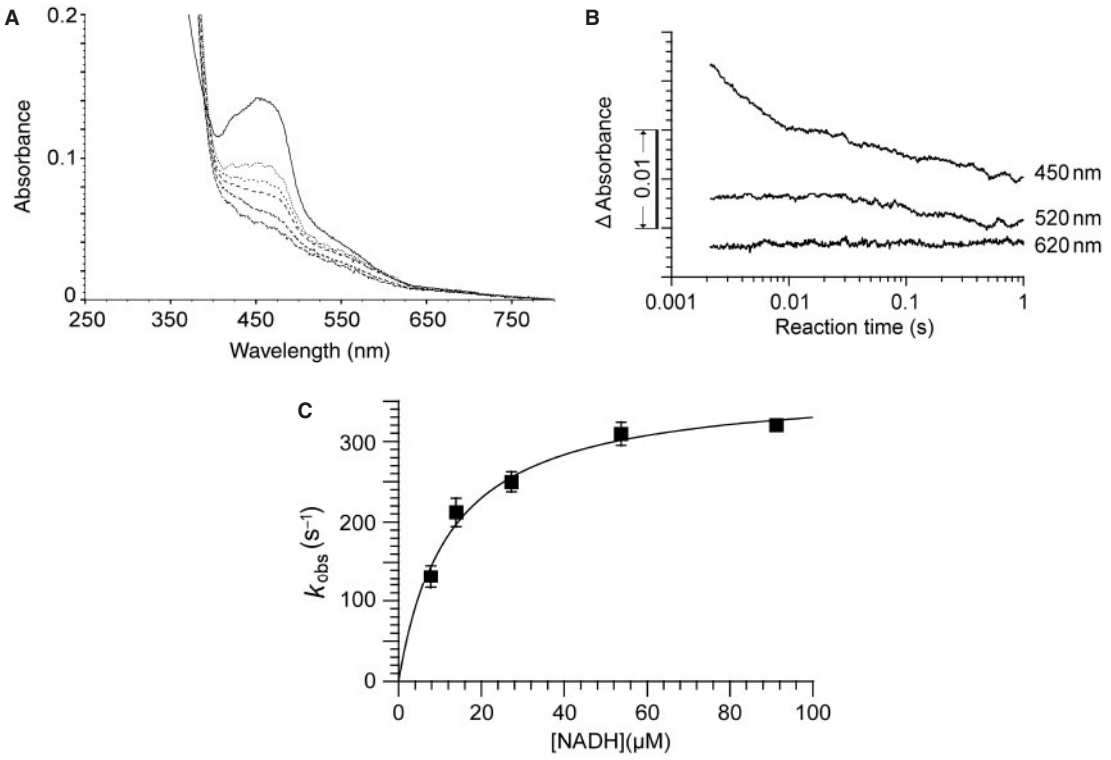

Fig. 2. **Changes of the absorption spectra of DTT-treated W335A/F336L mutant after mixing with NADH under anaerobic conditions**. (A) A 4.63 μM DTT-treated double mutant in 50 mM KP buffer (pH 7.8) containing 0.4 mM EDTA was anaerobically mixed with 1/39 volume of NADH (5.08 mM) in the same buffer, and the absorption spectra were recorded before mixing and at several times after mixing (20 s, 30 s, 60 s, 5 min and 60 min). (B) Time courses of absorption at 450, 520 and 630 nm of the mutant after mixing with 60 μM NADH using a stopped-flow apparatus. (C) Observed rate constants (k_{obs}) for the

XO (*26*), and a small amount of the neutral FAD semiquinone (FADH*) could be observed. To investigate this in more detail, we examined the reaction with the help of a stopped-flow spectrophotometer. Anaerobic mixing of DTT-treated mutant enzyme with NADH resulted in a triphasic reaction within 1 s (Fig. 2B). In the first phase (within 0.01 s), the absorbance at 450 nm rapidly decreased to ~40% of the level of the total change observed after 1 s, but the absorbance at 520 and 620 nm did not change within this first phase. This finding suggests that only FAD was reduced in the first phase, in contrast to the behaviour of native chicken liver XDH (*40*) or bovine milk XDH (*41*). Figure 2C shows the saturation curve with NADH as the substrate; double-reciprocal plots provided values of 370 ± 17/s and 12.2 ± 1.9 μM for k_{lim} and K_d, respectively, indicating that NADH is not tightly bound to the enzyme compared with other XDHs (*40*, *41*). In the second phase, the absorbance at 450 nm continued to decrease slightly, albeit more slowly, and the absorbance at 520 and 620 nm still showed no change. In the third phase, the absorbance at 450 nm was further decreased slightly, but the absorbance at 520 nm decreased and that at 620 nm increased. This indicates that there was an internal electron transfer that resulted in the formation of FADH* and reduction of the iron–sulphur cluster Fe/S II (*10*). Between 1 s and 20 s (Fig. 2A), no further major spectral changes were observed. The interpretation of these results will be discussed in more detail in the Discussion section.

Table 2. **Data collection and refinement statistics for the W335A, F336L double mutant of rat xanthine oxidoreductase.**

Space group	$P2_12_12_1$
Unit cell axes (Å)	a = 101.1 b = 139.5 c = 222.3
Resolution (Å)	25 – 2.28 (2.32 – 2.28)¶
Wavelength of data collection (Å)	1.000
Total number of reflections measured	1179,948
Number of unique reflections*	137,504
(Number of reflections used in R_{free})	5556
Completeness (%)	100 (100)¶
R_{sym}#	8.0 (38.7)¶
R_{cryst}* (%)	18.5 (20.9)¶
R_{free}† (%)	22.9 (28.4)¶
Deviations in bond lengths (Å)	0.008
Deviations in bond angles, degree	1.4
Average B-value (Å^2)	32.4
Number of non-hydrogen atoms	21,443
Number of water molecules	1391
Ramachandran plot (%)	88.2/10.8/0.7/0.3

¶Numbers in parentheses are for the highest resolution shell.
#$R_{sym} = \sum_{hkl}\sum_I |I_I - \langle I \rangle| / \sum_{hkl}\sum_I \langle I \rangle$.
*$R_{cryst} = \sum_{hkl} |F_{obs} - F_{calc}| / F_{obs}$.
†$R_{free} = R_{cryst}$ for 4.0% of randomly selected reflections not used in refinement.
The Ramachandran plot indicates the percentage of residues in the most favourable region, in the additionally allowed region, in the generously allowed region, and in the disallowed region. The Ramachandran plot was calculated by the program PROCHECK (*45*).

The Structure of the W335A/F336L Double Mutant Enzyme—The crystal structure of the mutant was determined in its demolybdo form at 2.3 Å resolution (Table 2). The crystal contained the functional dimer in the asymmetric unit. The overall chain trace is shown in Fig. 3A. The model has good overall stereochemistry with 88% of all residues in the most favourable regions of the Ramachandran plot. The residues in disallowed regions (Asp4 of chain A, Tyr152, Asp658 and Asn887 in all chains) are defined in $2F_o$–F_c electron density maps. For residues 1–2, 166–190 and 1319–1331, no corresponding electron density was observed, an indication of inherent flexibility.

The structures of the two subunits were quite similar, but not identical. The inter-domain linker (residues 532–589) between the FAD and the molybdopterin domain in subunit A can be observed in the electron density map, in contrast to previous XDH and XO structures (*6*). The conformation is almost identical to that of the corresponding stretch of amino acids in the rat XDH C535A/C992R/C1324S triple mutant that does not convert from XDH to XO, and is the only other XDH/XO structure with a fixed conformation for this part of the protein (*25*) (PDB ID 1WYG). Residues 532–539 and 548–553, part of the inter-domain linker in subunit B, were disordered. The observation of differing chain traces in the two subunits suggests high mobility of these regions in solution.

The amino acid clusters that play a crucial role in the XDH/XO conversion (*26*) were also not identical in their conformations (Fig. 4A and B). The cluster formed by the four residues Arg334, Trp335, Arg426 and Phe549 is tightly packed in the XDH forms of both the native enzyme (*6*, *26*) and triple mutant (*25*) (Fig. 4C). In subunit A, electron density corresponding to the side chains of Phe549 and Arg334 was weak, but the backbone density was continuous and clear (Fig. 5A). In contrast, no electron density corresponding to Phe549 or the side chain of Arg334 could be observed in subunit B (Fig. 5B). The distances between the alpha-carbons of Arg426 and Arg334 are 20.1 and 20.2 Å in subunits A and B, respectively, whereas only 9.2 Å separates the two residues in the XDH form of the rat triple mutant. This suggests that the packing of the cluster is quite loose in this mutant; in solution, most of the cluster will be disrupted and only a small part of the molecules will have the four residues associated. Arg426, which is also part of the active site loop, has shifted its position in both subunits. The chain trace of the active site loop in this mutant is very similar to that of bovine XO (*6*) (PDB ID 1FIQ). The re-arrangement of the active site loop causes structural changes around FAD, blocking the approach of NAD^+ (Fig. 3B and C).

In bovine XOR, the electrostatic environments of XDH and XO differ dramatically. In the XDH form, the carboxylate of Asp429 (corresponds to Asp428 in rat enzyme) is close to the C6 carbon of FAD. In the XO form, this residue moves away from FAD and the guanidino group of Arg426 (Arg425 in rat) takes up a

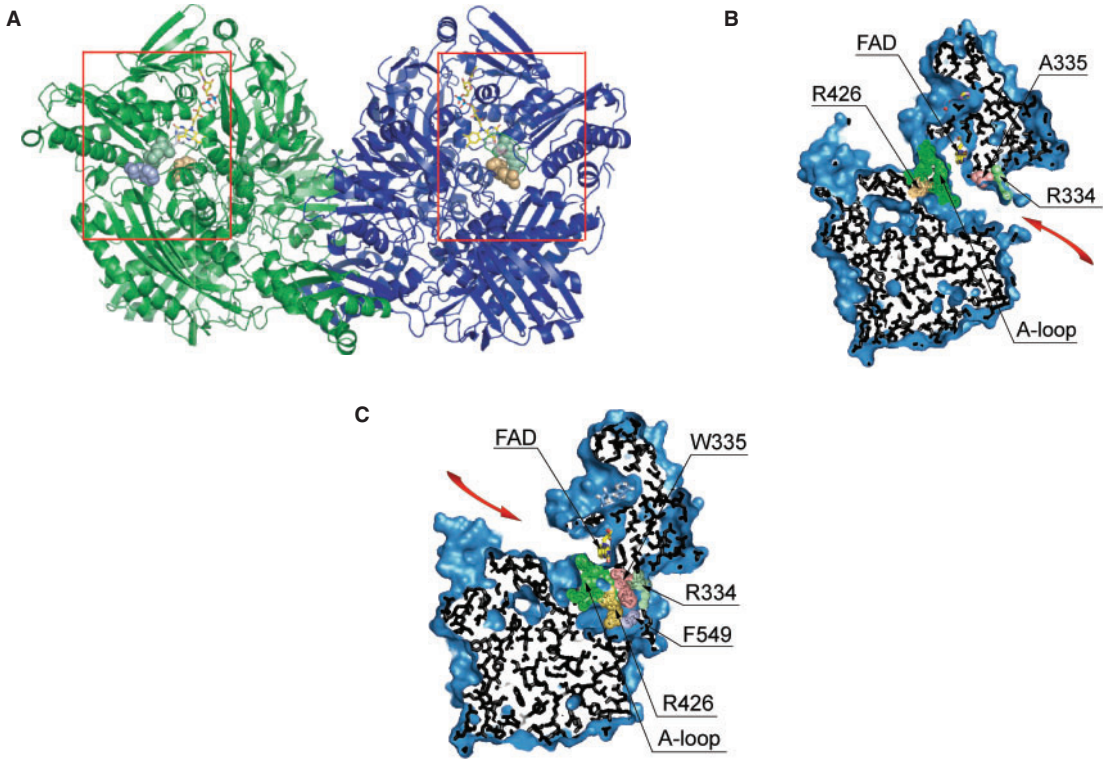

Fig. 3. **Structural consequences of the W335A/F336L mutation of rat XOR.** (A) Overall structure of the rat W335A/F336L mutant. Subunit A is shown in green and subunit B in blue. Red boxes mark the regions of each subunit shown in higher magnification in Fig. 4A and B. (B) In the XO form (e.g. subunit B of the W335A/F336L mutant), the cluster has disintegrated and opened up another access route (red arrow) to the flavin ring from the opposite side of the molecule. At the same time, the NAD^+-binding site has been partially filled-in, preventing access of this substrate. The residues 334, 335 and 426 are shown in space-filling representation; FAD is shown in stick representation; the active site loop (A-loop) is in space-filling representation (green). (C) In the XDH form (e.g. in the C535A/C992R/C1324S triple mutant), the enzyme molecule displays the elongated cleft (red arrow) necessary for binding of the substrate NAD^+. Note the compactness of the cluster. The cluster consisting of residues 334, 335, 426 and 549 is shown in space-filling representation; FAD is shown in stick

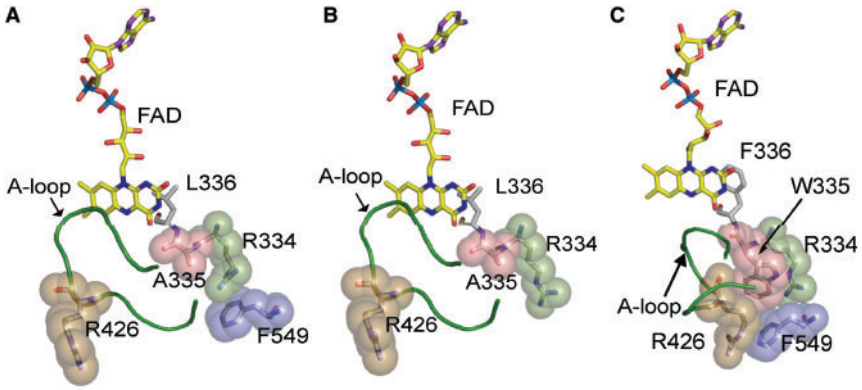

Fig. 4. **The residues of the cluster and active site loop in W335A/F336L mutant of rat XOR**. In all figures, the cluster consisting of residues 334, 335, 426 and 549 is shown in stick and space-filling representation; residue 336 and FAD are shown in stick representation only; the active site loop (A-loop) is in green. (A) Subunit A of the W335A/F336L mutant (B) Subunit B of the W335A/F336L mutant (C) The corresponding region of the XDH-locked C535A/C992R/C1324S triple mutant of the rat enzyme (*25*) has the cluster in the closed conformation and is shown for comparison.

similar position. These changes have been suggested as the reason for the observed modulation of the reactivity of the FAD cofactor. Equivalent changes were observed in the structure presented here. In the XDH-locked rat triple mutant, the carboxyl carbon of Asp428 is located 4.2 Å away from the C6 carbon of FAD. In the W335A/F336L mutant, however, the guanidino group of Arg425 approaches C6 at a distance of 6.3 Å.

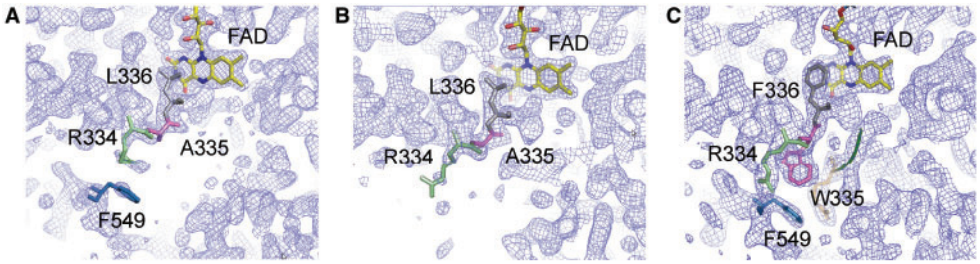

Fig. 5. **Electron density corresponding to the residues of the cluster and active site loop in W335A/F336L mutant of rat XOR**. These residues are represented in the same colours as in Fig. 4, but from different orientations. (A) Electron density in subunit A, (B) electron density in subunit B and (C) electron density in the C535A/C992R/C1324S triple mutant.

Another difference between the XDH-locked triple mutant and the W335A/F336L mutant is the change of orientation of the hydroxyl groups of the flavin ribitol chain. In the XDH triple mutant, the 2′-hydroxyl group forms a hydrogen bond to the side chain of Thr261. In the present double mutant, however, the same 2′-hydroxyl group hydrogen bonds to the carbonyl oxygen of Asp350, with the 3′-hydroxyl now interacting with Thr261 (Fig. 6A and B).

In both subunits, there was no electron density representing the C-terminal regions of the protein chains, which consequently seem to be mobile. In the mutant, the side chain of Leu336 was located at the same position as the benzene ring of Phe336 of the XDH type triple mutant (*25*). The structures of the Fe/S domain and the molybdopterin domain are very similar to those of the rat XDH triple mutant, i.e. the standard fold established for the bovine enzyme (*6*).

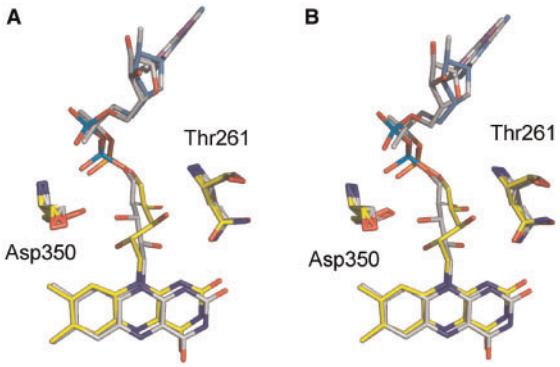

Fig. 6. **The orientation of the hydroxyl groups of the flavin ribitol chain.** Flavin cofactor in subunit A (A) or subunit B (B) of the rat W335A/F336L mutant (yellow) was compared to that in the XDH-locked C535A/C992R/C1324S triple mutant (grey) of the rat enzyme. These structures were superimposed on the molybdopterin and Fe/S domains. In the double mutant, the 2′ and 3′-hydroxyl groups of flavin ribitol are in different orientations from those in the XDH triple mutant.

DISCUSSION

The features of the mutant presented in this article are consistent with the previous suggestion that the amino acid cluster identified by Kuwabara *et al*. (*26*) plays a key role in the XDH/XO transition; it not only acts as a transmitter of the signals induced by the formation of the Cys535–Cys992 disulphide, or by proteolytic cleavage of the peptide linking the FAD and molybdopterin domains, to the active site, leading to conformational changes around FAD, but also acts as a solvent gate (Figs 3B and 4). In their model, tight interactions between the amino acid residues of the cluster should be crucial for the stabilization of the XDH form of the enzyme. With the native enzyme, the disruption of the cluster seems to be initiated by the removal of Phe549, caused by a change in conformation induced either by disulphide formation or by proteolysis within the inter-domain linker peptide. In this study, we disrupted the cluster by mutation of W335 to alanine. As predicted, the enzyme was expressed mostly in its XO form, mainly displaying oxidase activity, even though it can partly acquire dehydrogenase activity through incubation with DTT.

In the crystal structure of the DTT-treated form of the W335A/F336L mutant, several residues assumed different positions in the two subunits. This is indicative of high mobility of these parts of the protein (Figs 4A, B, 5A and B). Although the two subunits are not identical, the active site loop of the double mutant was located on the *si*-side of the FAD cofactor, as found in the native XO (Fig. 4A and B), and the solvent gate was essentially open in both (*26*) (Figs 3B, 4A and B). However, in subunit B the cluster was completely disrupted, whereas in subunit A it was still partly associated, although Phe549 and Arg334 are only represented by rather weak electron density. Crystal packing forces always have to be considered when interpreting such results; however, we feel the fact that the two subunits are asymmetric reflects the low but significant XDH activity that the enzyme acquires after DTT treatment. In solution, the mutant protein is probably constantly shifting between XO and XDH conformations. In the untreated enzyme, the ratio between the two forms is greatly in favour of the XO form. DTT treatment, however, will restore the pyridine nucleotide binding site, at least in part, leading to an increase in the enzyme's XDH activity. During purification, the double mutant is converted more easily to the XO form than the native enzyme because the destabilization of the cluster by the loss of the tryptophan side chain allows faster disulphide formation.

When the enzyme was incubated with DTT, the gain of xanthine–NAD^+ activity was less than the loss of xanthine–O_2 activity. This result can be explained by

the positive shift of the redox potential of the FAD cofactor caused by replacing F336 with a leucine, leading to the loss of stacking interaction between the aromatic ring of F336 and the isoalloxazine middle ring. This idea is supported by the increase in electron acceptance observed when $ACPY^+$, an NAD^+ analogue with a more positive redox potential, is used. The limited number of accessible NAD^+-binding sites has a negative influence on both oxidation and reduction of the NAD^+ substrate. The shift in redox potential, however, makes NADH a good electron donor for this mutant, although only FAD was reduced in the first rapid phase of the reaction with lower binding affinity compared to the native XDH from chicken liver or bovine milk (*40*, *41*). The second slower phase of FAD reduction may reflect the possible shift in equilibrium between XO and XDH conformations after reduction of the XDH form with NADH. After that, slower electron transfer occurred to form only a small amount of $FADH^*$ with partial reduction of one of the iron–sulphur centres, most likely FeS/II (*10*). The amount of reduced FAD cofactor in the fast phase may correspond to the amount of XDH conformation accessible to the mutant in solution. Only very little further reduction can be achieved due to the higher redox potential of the FAD cofactor compared to the Fe/S II cluster.

The most striking and potentially useful feature of the W335A/F336L mutant is its ability to produce a much higher ratio of O_2^-, regardless of potential DTT treatment and the presence of pyridine nucleotides, i.e. of the redox state of its environment. The mutant can achieve this because its conformation is strongly shifted towards the XO form and its FAD redox potential is higher than that of the normal enzyme. In the present catalytic model, O_2^- is formed by the reaction of $FADH^*$ with molecular oxygen; $FADH^*$ is thought to be either thermodynamically stable or kinetically accessible during turnover. In native XOR, the redox potentials of the cluster Fe/S II and of FAD are not far apart and are in thermodynamic equilibrium, so the FAD cofactor exists in both the $FADH_2$ and $FADH^*$ states that lead to H_2O_2 and O_2^-, respectively, when reacting with oxygen (*42*, *43*). Under these conditions, FAD's redox potential shifts to a higher value, and during turnover FAD can receive one electron from Fe/S II to form $FADH^*$, which in turn reacts readily with the oxygen substrate to form O_2^-. A similar scenario might be in play when the deflavo enzyme is reconstituted with 4-thio FAD (*44*) or 7-Cl FAD (Nishino, T and Massey, V, unpublished observation). These compounds' redox potentials are much higher than that of Fe/S II and, consequently, they produce large amounts of O_2^-.

Even without a complete understanding of the mechanism of formation of O_2^-, the W335A/F336L mutant should prove very valuable as an experimental tool. Its relative ease of preparation, stability and high superoxide yield, as well as the absence of any requirement for additional complex protein factors, represent a major improvement over existing superoxide-generating systems such as NADPH oxidases (*27*). Expression of the mutant gene in cells will provide a convenient method to observe the effects of transient or persistent increases in O_2^- concentrations on cellular phenomena.

We thank SPring-8 for beamtime and the staffs of beamline BL38B1 for their support during data collection. This work was supported by Grants-in-Aid (T.N. 16205021) for Science Research from the Ministry of Education, Science, Sports and Culture of Japan as well as by a grant from the Canadian Institute of Health Research and the Canada Research Chairs Program (EFP). The atomic coordinates and structure factors (code 2E3T) have been deposited in the Protein Data Bank.

REFERENCES

1. Bray, R.C. (1975) Molybdenum iron-sulfur flavin hydroxylases and related enzymes in *The Enzymes.* (Boyer, P.D., ed.) Vol. XII, Part B, 3rd edn. pp. 299–419 Academic Press, New York and London
2. Nishino, T. (1994) The conversion of xanthine dehydrogenase to xanthine oxidase and the role of the enzyme in reperfusion injury. *J. Biochem.* **116**, 1–6
3. Hille, R. and Nishino, T. (1995) Flavoprotein structure and mechanism. 4. Xanthine oxidase and xanthine dehydrogenase. *FASEB J.* **9**, 995–1003
4. Amaya, Y., Yamazaki, K., Sato, M., Noda, K., Nishino, T., and Nishino, T. (1990) Proteolytic conversion of xanthine dehydrogenase from the NAD-dependent type to the O2-dependent type. Amino acid sequence of rat liver xanthine dehydrogenase and identification of the cleavage sites of the enzyme protein during irreversible conversion by trypsin. *J. Biol. Chem.* **265**, 14170–14175
5. Sato, A., Nishino, T., Noda, K., Amaya, Y., and Nishino, T. (1995) The structure of chicken liver xanthine dehydrogenase. cDNA cloning and the domain structure. *J. Biol. Chem.* **270**, 2818–2826
6. Enroth, C., Eger, B.T., Okamoto, K., Nishino, T., Nishino, T., and Pai, E.F. (2000) Crystal structures of bovine milk xanthine dehydrogenase and xanthine oxidase: structure-based mechanism of conversion. *Proc. Natl. Acad. Sci. USA* **97**, 10723–10728
7. Olson, J.S., Ballou, D.P., Palmer, G., and Massey, V. (1974) The mechanism of action of xanthine oxidase. *J. Biol. Chem.* **249**, 4363–4382
8. Kobayashi, K., Miki, M., Okamoto, K., and Nishino, T. (1993) Electron transfer process in milk xanthine dehydrogenase as studied by pulse radiolysis. *J. Biol. Chem.* **268**, 24642–24646
9. Hille, R. (1996) The mononuclear molybdenum enzymes. *Chem. Rev.* **96**, 2757–2816
10. Nishino, T. and Okamoto, K. (2000) The role of the [2Fe-2s] cluster centers in xanthine oxidoreductase. *J. Inorg. Biochem.* **82**, 43–49
11. Komai, H., Massey, V., and Palmer, G. (1969) The preparation and properties of deflavo xanthine oxidase. *J. Biol. Chem.* **244**, 1692–1700
12. Corte, E.D. and Stirpe, F. (1968) Regulation of xanthine oxidase in rat liver: modifications of the enzyme activity of rat liver supernatant on storage at 20 degrees. *Biochem. J.* **108**, 349–351
13. Stirpe, F. and Della Corte, E. (1969) The regulation of rat liver xanthine oxidase. Conversion in vitro of the enzyme activity from dehydrogenase (type D) to oxidase (type O). *J. Biol. Chem.* **244**, 3855–3863
14. Corte, E.D. and Stirpe, F. (1972) The regulation of rat liver xanthine oxidase. Involvement of thiol groups in the conversion of the enzyme activity from dehydrogenase (type D) into oxidase (type O) and purification of the enzyme. *Biochem. J.* **126**, 739–745
15. Waud, W.R. and Rajagopalan, K.V. (1976) Purification and properties of the NAD+-dependent (type D) and O2-dependent (type O) forms of rat liver xanthine dehydrogenase. *Arch. Biochem. Biophys.* **172**, 354–364

16. Nakamura, M. and Yamazaki, I. (1982) Preparation of bovine milk xanthine oxidase as a dehydrogenase form. *J. Biochem. (Tokyo)* **92**, 1279–1286
17. Saito, T. and Nishino, T. (1989) Differences in redox and kinetic properties between NAD-dependent and O2-dependent types of rat liver xanthine dehydrogenase. *J. Biol. Chem.* **264**, 10015–10022
18. Hunt, J. and Massey, V. (1992) Purification and properties of milk xanthine dehydrogenase. *J. Biol. Chem.* **267**, 21479–21485
19. Nishino, T. and Nishino, T. (1997) The conversion from the dehydrogenase type to the oxidase type of rat liver xanthine dehydrogenase by modification of cysteine residues with fluorodinitrobenzene. *J. Biol. Chem.* **272**, 29859–29864
20. Jarasch, E.D., Grund, C., Bruder, G., Heid, H.W., Keenan, T.W., and Franke, W.W. (1981) Localization of xanthine oxidase in mammary-gland epithelium and capillary endothelium. *Cell* **25**, 67–82
21. McCord, J.M. and Roy, R.S. (1982) The pathophysiology of superoxide: roles in inflammation and ischemia. *Can. J. Physiol. Pharmacol.* **60**, 1346–1352
22. McCord, J.M. (1985) Oxygen-derived free radicals in post-ischemic tissue injury. *N. Engl. J. Med.* **312**, 159–163
23. Saugstad, O.D. (1988) Hypoxanthine as an indicator of hypoxia: its role in health and disease through free radical production. *Pediatr. Res.* **23**, 143–150
24. Berry, C.E. and Hare, J.M. (2004) Xanthine oxidoreductase and cardiovascular disease: molecular mechanisms and pathophysiological implications. *J. Physiol.* **555**, 589–606
25. Nishino, T., Okamoto, K., Kawaguchi, Y., Hori, H., Matsumura, T., Eger, B.T., Pai, E.F., and Nishino, T. (2005) Mechanism of the conversion of xanthine dehydrogenase to xanthine oxidase: identification of the two cysteine disulfide bonds and crystal structure of a non-convertible rat liver xanthine dehydrogenase mutant. *J. Biol. Chem.* **280**, 24888–24894
26. Kuwabara, Y., Nishino, T., Okamoto, K., Matsumura, T., Eger, B.T., Pai, E.F., and Nishino, T. (2003) Unique amino acids cluster for switching from the dehydrogenase to oxidase form of xanthine oxidoreductase. *Proc. Natl. Acad. Sci. USA* **100**, 8170–8175
27. Vignais, P.V. (2002) The superoxide-generating NADPH oxidase: structural aspects and activation mechanism. *Cell. Mol. Life Sci.* **59**, 1428–1459
28. Grivennikova, V.G. and Vinogradov, A.D. (2006) Generation of superoxide by the mitochondrial Complex I. *Biochim. Biophys. Acta* **1757**, 553–561
29. Williamson, D.H., Lund, P., and Krebs, H.A. (1967) The redox state of free nicotinamide-adenine dinucleotide in the cytoplasm and mitochondria of rat liver. *Biochem. J.* **103**, 514–527
30. Ikegami, T. and Nishino, T. (1986) The presence of desulfo xanthine dehydrogenase in purified and crude enzyme preparations from rat liver. *Arch. Biochem. Biophys.* **247**, 254–260
31. Nishino, T., Amaya, Y., Kawamoto, S., Kashima, Y., Okamoto, K., and Nishino, T. (2002) Purification and characterization of multiple forms of rat liver xanthine oxidoreductase expressed in baculovirus-insect cell system. *J. Biochem. (Tokyo)* **132**, 597–606
32. Summers, M.D., and Smith, G.E. (1987) *A Manual of Methods for Baculovirus Vectors and Insect Cell Culture Procedures*, Texas Agricultural Experiment Station Bulletin No. 1555. College Station, TX.
33. Vialard, J., Lalumiere, M., Vernet, T., Briedis, D., Alkhatib, G., Henning, D., Levin, D., and Richardson, C. (1990) Synthesis of the membrane fusion and hemagglutinin proteins of measles virus, using a novel baculovirus vector containing the beta-galactosidase gene. *J. Virol.* **64**, 37–50
34. Nishino, T., Nishino, T., and Tsushima, K. (1981) Purification of highly active milk xanthine oxidase by affinity chromatography on sepharose 4B/folate gel. *FEBS Lett.* **131**, 369–372
35. Johnson, J.L., Waud, W.R., Cohen, H.J., and Rajagopalan, K.V. (1974) Molecular basis of the biological function of molybdenum. Molybdenum-free xanthine oxidase from livers of tungsten-treated rats. *J. Biol. Chem.* **249**, 5056–5061
36. McCord, J.M. and Fridovich, I. (1968) The reduction of cytochrome *c* by milk xanthine oxidase. *J. Biol. Chem.* **243**, 5753–5760
37. Massey, V. (1959) The microestimation of succinate and the extinction coefficient of cytochrome *c*. *Biochim. Biophys. Acta* **34**, 255–256
38. Strickland, S., Palmer, G., and Massey, V. (1975) Determination of dissociation constants and specific rate constants of enzyme-substrate (or protein-ligand) interactions from rapid reaction kinetic data. *J. Biol. Chem.* **250**, 4048–4052
39. Hermes, J.D., Morrical, S.W., O'Leary, M.H., and Cleland, W.W. (1984) Variation of transition-state structure as a function of the nucleotide in reactions catalyzed by dehydrogenases. 2. Formate dehydrogenase. *Biochemistry* **23**, 5479–5488
40. Schopfer, L.M., Massey, V., and Nishino, T. (1988) Rapid reaction studies on the reduction and oxidation of chicken liver xanthine dehydrogenase by the xanthine/urate and NAD/NADH couples. *J. Biol. Chem.* **263**, 13528–13538
41. Hunt, J. and Massey, V. (1994) Studies of the reductive half-reaction of milk xanthine dehydrogenase. *J. Biol. Chem.* **269**, 18904–18914
42. Nishino, T., Nishino, T., Schopfer, L.M., and Massey, V. (1989) The reactivity of chicken liver xanthine dehydrogenase with molecular oxygen. *J. Biol. Chem.* **264**, 2518–2527
43. Harris, C.M. and Massey, V. (1997) The reaction of reduced xanthine dehydrogenase with molecular oxygen. Reaction kinetics and measurement of superoxide radical. *J. Biol. Chem.* **272**, 8370–8379
44. Nishino, T., Nishino, T., Schopfer, L.M., and Massey, V. (1989) Reactivity of chicken liver xanthine dehydrogenase containing modified flavins. *J. Biol. Chem.* **264**, 6075–6085
45. Laskowski, R.A., MacArthur, M.W., Moss, D.S., and Thornton, J.M. (1993) Procheck: a program to check the stereochemical quality of protein structures. *J. Appl. Crystallogr.* **26**, 283–291